Trion fine structure and anomalous Hall effect in monolayer transition metal dichalcogenides

A. Hichri *

Laboratoire de Physique des Matériaux Structure et Propriétés, Faculté des Sciences de Bizerte, Université de Carthage, 7021 Zarzouna, Tunisie

S. Jaziri

Laboratoire de Physique de la Matière Condensée, Faculté des Sciences de Tunis, Université de Tunis El Manar, 2092 El Manar, Tunisie

(Received 25 February 2020; revised 11 July 2020; accepted 21 July 2020; published 6 August 2020)

We theoretically investigate two spin configurations of a negative trion in monolayer tungstenides, called the intravalley spin singlet and intervalley spin triplet. The energy splitting between them is attributed to the trion fine structure, arising from the electron-hole exchange interaction. Using the Rytova-Keldysh potential, we show that the splitting which acts as an effective Zeeman effect is tuned by varying the dielectric environment. For the negative trion in the WSe_2 monolayer encapsulated in hexagonal boron nitride, the calculated splitting is around 6 meV, which is in agreement with recent experiments. Owing to the strong exchange, we show that the negative intervalley trion acquires a giant Berry curvature. This valley pseudospin-dependent Berry curvature largely dominates the intrinsic Berry curvature arising from the Bloch bands. An in-plane applied electric field gives rise to an anomalous valley Hall transport. We investigate the dependence of the anomalous Hall conductivity and magnetization on several parameters such as dielectric screening length and doping. The trion Hall effect can be considered as the basis for valley-based electronics applications.

DOI: 10.1103/PhysRevB.102.085407

I. INTRODUCTION

Transition metal dichalcogenide (TMDC) monolayers (MLs) are atomically thin semiconductors with the chemical formula MX_2, where M stands for the transition metal element Mo or W and X stands for the chalcogen element S or Se. MX_2 MLs have attracted enormous research interest due to their distinctive electronic and optical properties [1–16]. The inversion symmetry breaking, the spin-orbit coupling, and the strong electron-hole interaction are the most interesting features of TMDC MLs. The broken inversion symmetry leads to the formation of a direct band gap at the K and K' valleys [17], which are related by the time reversal operation. The strong spin-orbit coupling lifts the spin degeneracy of the energy bands. This spin splitting in K and K' must be opposite owing to time reversal symmetry, resulting in spin-valley locking. Accordingly, the combination of broken inversion symmetry with time reversal symmetry leads to valley-dependent optical selection rules [1,18]. The strong Coulomb interaction between the hole and the electron leads to their binding into a hydrogenlike bound pair, called an exciton. The exceptionally large exciton binding energy of several hundred meV [17,19–23] is due to the reduced screening effect, strong two-dimensional (2D) quantum confinement, and the large effective mass of the carriers. In a negatively (positively) doped sample, the bound electron-hole pair can capture an excess electron (hole) to form a negatively (positively) charged exciton, called the negative (positive) trion [8,12,14,17,22,24–27].

Excitons and trions comprise spin-/valley-polarized electrons and holes in the K and K' valleys, where the selection rules of optical transitions require the same spin and valley states of the electrons at the conduction and valence band edges. The intravalley (intervalley) excitons correspond to conduction and valence electrons residing in the same (opposite) valley. Due to the spin-orbit splitting of the conduction band Δ_{so}, we have two intravalley bright (singletlike) excitons at E_X and two intravalley spin-forbidden (tripletlike) dark excitons at $E_X - \Delta_{so}$. Four dark intervalley exciton states are possible (two at E_X and two at $E_X - \Delta_{so}$). Bright and dark trions have optical selection rules determined by their recombining electron-hole pair; that is, when the excess electron is bound to the bright (dark) exciton, the negative trion is bright (dark). We have therefore only four bright trion states: two intravalley trions and two intervalley trions. The experimental spectrum of the so-called darkish ML WX_2, shows the existence of a doublet attributed to intravalley and intervalley negative trions [8,14,28,29]. The two peaks are separated by a splitting $\delta^{exch} \sim 6$ meV [8,14,30–32], induced by electron-hole exchange interactions. The first peak corresponds to the intravalley negative trion which is observed even at ambient conditions, whereas the second emission, relative to the intervalley trion, is efficient only at low temperatures [14,30,33].

Other interesting properties have been observed for valley trions in ML WX_2 owing to the presence of the Berry curvature, which arises from the dependence of the periodic part of the Bloch function on the trion center-of-mass wave vector. In crystals with inversion symmetry breaking, such

*aida.hichri@ipeib.u-carthage.tn

as ML TMDCs, electrons in the K and K' valleys have opposite Berry curvatures [34,35]. In momentum space, the Berry curvature acts as an effective magnetic field [36]. The Berry curvature and the orbital moment represent the effect of the Berry phase of electrons in the Bloch bands [37]. For intervalley negative trions in ML WX_2, in addition to the Berry curvature inherited from Bloch functions, these trions acquire a giant Berry curvature arising from the electron-hole exchange interaction [38,39]. The finite Berry curvature leads to nontrivial spin/valley transport. By applying an in-plane electric field, transverse responses have been observed in charge, spin, and valley degrees of freedom of the Bloch electrons. Berry curvature generates an anomalous velocity that is perpendicular to the applied electric field [1,40]. Thereby, it describes spin and valley anomalous Hall effects [4,38]. The orbital moment arising from the self-rotating motion of the electron wave packet is responsible for the anomalous g factor of electrons in semiconductors [3]. The Berry curvature at the edges of the valence and conduction bands is more significant to photoexcited charge carriers; that is, when the charge carriers are generated by circular polarization, electrons and holes have anomalous Hall conductivity or magnetization even at zero magnetic field. The spatially and polarization-resolved photoluminescence (PL) can be used to detect the trion valley Hall effect. It is worth noting that the scattering between states with opposite Berry curvature will remove the Hall effect. In fact, for a negative trion the valley Hall effect is protected because the scattering is inefficient [4].

In this work, (i) we will study the splitting between intervalley and intravalley trions in ML WX_2 caused by the electron-hole exchange interaction, and (ii) we will investigate the anomalous Hall effects due to the giant Berry curvature resulting from the trion fine structure. This paper is organized as follows: in Sec. II, we use the 2D effective-mass approximation to study the optical properties of the inter- and intravalley trions in ML WX_2. In order to estimate the magnitude order of the energy splitting observed between these two entities, a detailed analysis of trion fine structure is needed. In Sec. III, we discuss the trion transport properties, and we show that the giant Berry curvature arising from the electron-hole exchange introduces a large valley Hall effect. Finally, in the last section we present our conclusions.

II. TRION OPTICAL PROPERTIES

In the center-of-mass frame, the trion Hamiltonian can be written as the sum of three Hamiltonians: $H = H_{\rm cm} + H_{\rm rel} + H_{\rm exch}$. The first term, $H_{\rm cm} = (\hbar^2 k^2/2M)$, is the kinetic energy of the negative (positive) trion center-of-mass motion, where $\mathbf{k}$ and $M = 2m_{e(h)} + m_{h(e)}$ are the center-of-mass wave vector and mass, respectively. The second term corresponds to the relative Hamiltonian, and the third one corresponds to the trion exchange Hamiltonian. We start with the resolution of the relative Hamiltonian.

A. Model

Using the 2D effective-mass approximation, the relative trion Hamiltonian is given by [8,22]

$$H_{\rm rel} = -\frac{\hbar^2}{2\mu}\frac{\partial^2}{\partial\rho_1^2} + V(\rho_1) - \frac{\hbar^2}{2\mu}\frac{\partial^2}{\partial\rho_2^2} + V(\rho_2) - \frac{\hbar^2}{\mu}\left(\frac{\sigma}{\sigma+1}\right)\frac{\partial}{\partial\rho_1}\frac{\partial}{\partial\rho_2} + V(|\boldsymbol{\rho_1} - \boldsymbol{\rho_2}|), \quad (1)$$

where $\mu = \frac{m_e m_h}{m_e + m_h}$ is the reduced effective mass and $\sigma = \frac{m_e}{m_h}$ ($\sigma = \frac{m_h}{m_e}$) is the effective mass ratio for the negative (positive) trion. $\boldsymbol{\rho}_1 = \boldsymbol{\rho}_{e1} - \boldsymbol{\rho}_h$, and $\boldsymbol{\rho}_2 = \boldsymbol{\rho}_{e2} - \boldsymbol{\rho}_h$, where $\boldsymbol{\rho}_{ei}$ (m_e) and $\boldsymbol{\rho}_h$ (m_h) are the in-plane position vectors (masses) for the electrons and the hole, respectively. $V(\rho)$ is the nonlocally screened electron-hole interaction originating from the change in the dielectric environment. This so-called Rytova-Keldysh potential is written as follows [41]:

$$V(\rho) = -\frac{\pi e^2 k_s}{(\varepsilon_{\rm sub} + \varepsilon_{\rm cap})}[H_0(\rho k_s) - Y_0(\rho k_s)], \quad (2)$$

where $H_0(x)$ and $Y_0(x)$ are the Struve function and Bessel function of the second kind, respectively. The parameter k_s explains the strong dielectric contrast between the ML and its surroundings; $\epsilon_{\rm sub}$ and $\epsilon_{\rm cap}$ are the relative dielectric constants of the substrate and cap layer, respectively.

In order to solve the eigenvalue equation of relative motion, we use a wave function expansion technique; it is factorized into [42]

$$\zeta_{X_-}(\rho_1, \rho_2) = \sum_{\tilde{n},\tilde{l}} D(\tilde{n}, \tilde{l})\frac{1}{\sqrt{2}}\{\phi_{\tilde{l}s}(\rho_1)\phi_{\tilde{n}\tilde{l}}(\rho_2) + \phi_{\tilde{l}s}(\rho_2)\phi_{\tilde{n}\tilde{l}}(\rho_1)\}. \quad (3)$$

Here, $\phi_{\tilde{n}\tilde{l}}(\rho_i) = \sum_{n,l} C(n,l)\varphi_{n,l}(\rho,\theta)$ is the wave function solution of the exciton Hamiltonian, expanded in terms of the 2D hydrogenic state $\varphi_{n,l}(\rho,\theta)$ (see Ref. [22] for more details). The number $\tilde{n}, \tilde{l}$ refers to the dominant contribution of the coefficients $C(n,l)$ to the excitonic function. The diagonalization of the Hamiltonian matrix leads to the following eigenvectors: $\Phi_{\rm rel}(\rho_1,\rho_2) = \sum_{i,j} c(i,j)\zeta_{X_-}(\rho_1,\rho_2)$ and eigenvalues $E_{\rm rel}$. By taking into account the trion center-of-mass energy $E_{\rm cm} = \hbar^2 k^2/2M$, the trion energies are given by $E_{Tn} = E_g + E_{\rm rel} + E_{\rm cm}$, where E_g is the band gap. The obtained negative-trion states are eightfold degenerate; four are dark, where the excess electron is bound to a dark exciton, and four are bright, where the excess electron is bound to a bright exciton. In order to explain the observed energy splitting between the two degenerate bright negative trions in ML WX_2 [8,14,30,43], we need to identify and resolve the exchange Hamiltonian which takes into account the different valley configurations. Consequently, a rigorous analysis of trion fine structure is needed.

B. Trion fine structure

The optical selection rules require the same spin and valley states of the involved electrons at the maximum of the conduction and valence bands [23,44]. For intravalley negative trions, the exciton and the excess electron reside in the same valley. The Pauli exclusion principle dictates that the two electrons must occupy different spin states and thus reside in the top and bottom spin-split conduction bands, respectively [8,23,42,45]. However, for intervalley bright negative trions, all the constituent particles must have the same spin orientation as they

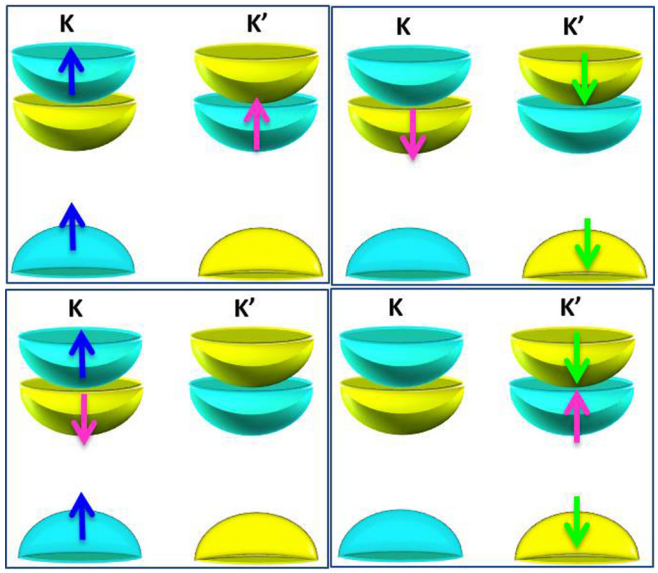

FIG. 1. The four valley configurations of bright negative trions distinguished by the valley pseudospin σ_z of the recombining electron-hole pair and the spin s_z of the excess electron (the magenta arrow). $\sigma_z = 1$ ($\sigma_z = -1$) on the left (right) side corresponds to the exciton pseudospin in the K (K') valley. Cyan and yellow hemispheres show the conduction and valence bands, and the arrow direction represents the spin direction. Top (Bottom): the two configurations of the bright intervalley (intravalley) trions.

differ in their valley index. In other words, in reference to the intravalley (intervalley) trion, the two electrons involved in the excitonic complex are characterized by antiparallel (parallel) alignment of their spins, thus forming a spin singlet (triplet) trion [8,14,28]. These two species, which differ in their spin configuration, can be distinguished by the bright exciton valley pseudospin index σ_z and the spin index s_z of the excess electron, as illustrated in Fig. 1. $\sigma_z = 1$ ($\sigma_z = -1$) denotes the exciton valley pseudospin up (down) in the K (K') valley which couples only to a σ_+ (σ_-) photon. The electron-hole exchange interaction couples the valley pseudospin to the trion center-of-mass wave vector.

For a negative trion in ML WX_2 there are eight exchange interaction processes. Four are summarized in the Supplemental Material [46]; the other four are deduced by time reversal symmetry. Accordingly, the negative-trion exchange Hamiltonian is $H_{\rm exch} = H_{e-h}^{\rm Intra} + H_{e-h}^{\rm Inter} + H_{X-e}$, where the intravalley electron-hole exchange $H_{e-h}^{\rm Intra}$ is independent of the exciton pseudospin σ_z and the spin index of the excess electron s_z, as shown in Fig. S1. By contrast, the intervalley electron-hole exchange $H_{e-h}^{\rm Inter}$ couples the two valleys, K and K'. This process engenders an annihilation of an electron-hole pair in the K valley and the creation of a pair in the K' valley, as shown in Fig. S2. This contribution can be written as [2,4] $H_{e-h}^{\rm Inter} = J_{e-h}^{\rm Inter}\sigma_+ + {\rm c.c.}$, where $J_{e-h}^{\rm Inter}$ is the strength of the electron-hole exchange interaction. The last Hamiltonian H_{X-e} originates from the interaction between the excess electron spin index in the K (K') valley and the pseudospin index of the recombining electron-hole pair, which resides necessary in the opposite valley K' (K). Consequently, H_{X-e} is zero (finite) for the intravalley (intervalley) trion where $\sigma_z s_z = -1$ ($\sigma_z s_z = 1$). Normally, H_{X-e} involves two contributions: the indirect electron-hole exchange and the electron-electron exchange interaction. Owing to the Coulomb repulsion the latter contribution is neglected, as summarized in the Supplemental Material. Therefore, this term can be written as [4,38] $H_{X-e} = (\sigma_z s_z + 1)\delta^{\rm exch}/2$. The exchange Hamiltonian of the negative trion in ML WX_2 can be expressed as follows [4,31,38]:

$$H_{\rm exch} = \left(\left|J_{e-h}^{\rm Intra}\right| + \frac{\delta^{\rm exch}}{2}\right) I + J_{e-h}^{\rm Inter}\sigma_+ + \left(J_{e-h}^{\rm Inter}\right)^{\dagger}\sigma_- + \sigma_z s_z \frac{\delta^{\rm exch}}{2}, \tag{4}$$

where the valley-orbit coupling strength, given by [4,47,48]

$$J_{e-h}^{\rm Inter} \sim -|\phi_{\tilde{1}s}(0)|^2 (at/E_g)^2 V(k) k^2 \exp(-2i\beta), \tag{5}$$

originates from the long-range part of the intervalley electron-hole exchange interaction. In contrast to $J_{e-h}^{\rm Inter}$, which leads to valley coupling, the pseudospin-independent term [38] $J_{e-h}^{\rm Intra} \sim |J_{e-h}^{\rm Inter}|$ gives rise to an overall shift of the trion energy. $|\phi_{\tilde{1}s}(0)|^2$ is the oscillator strength, i.e., the probability of finding the electron-hole in the same position [22,49], and $\beta = \arctan(k_y/k_x)$. t is the nearest-neighbor hopping integral, and a is the lattice constant [1]. In Eq. (4), $\delta^{\rm exch} \sim 0.1|\phi_{e-h}(0)|^2 V(K)$ represents the indirect electron-hole exchange interaction, where $K = \frac{4\pi}{3a}$ is the wave vector from the K point to the Γ point of the Brillouin zone (see the Supplemental Material). The splitting $\delta^{\rm exch}$ depends on K because it results from the electron-hole scattering with a large wave vector [4]. $\delta^{\rm exch}$ is finite for the top configurations shown in Fig. 1 and zero for the bottom configurations, where the spin orientation of the extra electron is opposite to the other two carriers. The predominantly exchange term is the main origin of the splitting between intravalley ($\sigma_z s_z = -1$) and intervalley ($\sigma_z s_z = 1$) trions; it acts like an in-plane Zeeman field.

In 2D spin space, the diagonalization of the Hamiltonian matrix given by Eq. (4) generates two eigenvalues:

$$E^{\varsigma}(k) = \frac{\delta^{\rm exch}}{2} + \left|J_{e-h}^{intra}\right| + \varsigma\xi(k), \tag{6}$$

where $\xi(k) = \frac{1}{2}\sqrt{(\delta^{\rm exch})^2 + 4|J_{e-h}^{inter}|^2}$ and $\varsigma = \pm$ is the band index. Finally, at $\mathbf{k} = 0$ the eigenenergies of the intervalley and intravalley trion solutions of the full Hamiltonian H are given, respectively, by $E^{inter} = E_{T1} + \delta^{\rm exch}$ and $E^{intra} = E_{T1}$, where E_{T1} is the trion ground energy obtained by the diagonalization of the relative Hamiltonian given by Eq. (1). Using the conventional Coulomb interaction $V(k) = 2\pi e^2/\varepsilon k$, the exchange terms J_{e-h}^{intra} and J_{e-h}^{inter} scale linearly with the wave vector $\mathbf{k}$. Crucially, due to the 2D character of the ML, the fundamental properties of the exciton (binding energy, Bohr radius, oscillator strength) are expected to be influenced by the dielectric screening. Consequently, in the following we use the nonhydrogenic electrostatic potential given by Eq. (2); in reciprocal space, it is written as follows:

$$V(k) = \frac{4\pi e^2}{(\varepsilon_{\rm sub} + \varepsilon_{\rm cap})k}\left(\frac{k_s}{k_s + k}\right). \tag{7}$$

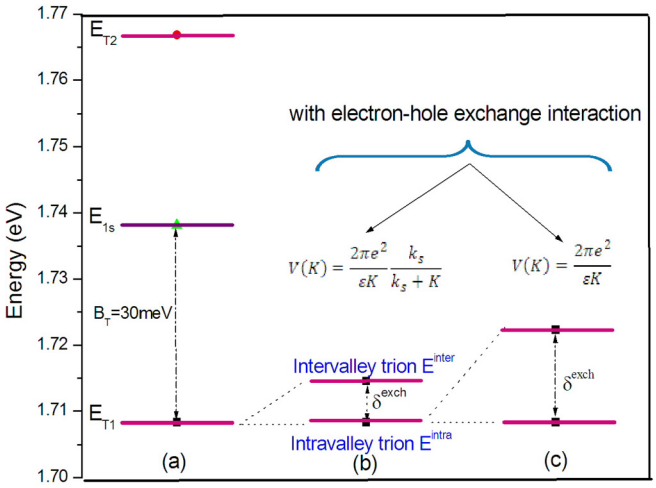

FIG. 2. Trion spectrum for WSe_2 ML encapsulated in hBN. (a) Ground and first excited states without trion fine structure. E_{1s} is the exciton ground state. By taking into account the trion fine structure a splitting δ^{exch} between intervalley and intravalley states is observed. δ^{exch} is calculated with (b) the Rytova-Keldysh potential and (c) the conventional Coulomb interaction.

The asymptotic behavior of the screening potential is $V(k) = \frac{2\pi e^2}{\varepsilon k}$ at $k_s \to \infty$, where $\varepsilon = (\varepsilon_{\text{sub}} + \varepsilon_{\text{cap}})/2$ is the average dielectric constant of the surrounding material.

For a WSe_2 layer encapsulated in hexagonal boron nitride (hBN) where $\varepsilon_{\text{sub}} = \varepsilon_{\text{cap}} = 3.3$ [8], the ground state and the first excited state of the trion at $\mathbf{k} = 0$ are plotted in Fig. 2(a). The trion binding energy B_T, which is conventionally introduced as $B_T = E_{1s} - E_{T1}$, is about 30 meV, where $E_{1s} = 1.73$ eV is the exciton ground state [22]. These results coincide with the experimental measurements. By taking into account the electron-hole exchange interaction, δ^{exch} leads to the splitting between intervalley and intravalley states at $\mathbf{k} = 0$. Using the Rytova-Keldysh (conventional Coulomb) potential, the splitting shown in Fig. 2(b) [Fig. 2(c)] is about 6 meV ($\delta^{\text{exch}} \sim 15$ meV). The obtained splitting $\delta^{\text{exch}} \sim 6$ meV is in agreement with experimental values using a high-quality hBN-encapsulated WSe_2 ML [8]. The calculated splitting with the conventional Coulomb potential is far from the experimental finding. The overall effect of the trion fine structure is a splitting of the four bright trion ground states E_{T1} into two degenerate states. The upper one corresponds to the intervalley trion E^{inter}, and the lower one corresponds to the intravalley trion E^{intra}, separated by the energy splitting δ^{exch}. The screening parameter k_s determines the band gap width δ^{exch}. As an example, for $k_s = 0.1$ Å^{-1}($r_s = 10$ Å) we obtain $\delta^{\text{exch}} = 3.9$ meV [43], and for $k_s = 0.15$ Å^{-1}($r_s = 6.4$ Å)[8] the splitting is $\delta^{\text{exch}} = 6$ meV. The decrease in the gap with decreasing k_s can be explained by the decreasing of the exchange interaction effect due to the screening caused by the change in the dielectric environment.

We can conclude that the trion fine structure leads to a splitting between intervalley and intravalley states, which was estimated to be on the order of 6 meV for WSe_2 using the Rytova-Keldysh potential given by Eq. (7). The splitting depends not only on μ, ε_{sub}, ε_{cap}, and k_s but also on the exact

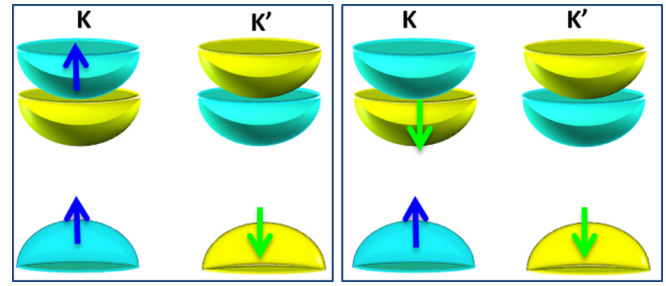

FIG. 3. Schematic configuration of the positive trions. The blue (green) arrows in the cyan (yellow) hemispheres represent the spin-up (spin-down) orientation for electrons in the conduction and valence bands.

form of the potential $V(\rho)$, which is sensitive to the details of the dielectric environment and the choice of substrate material. In the next section we will show that the trion fine structure plays an important role in transport properties.

III. TRION TRANSPORT PROPERTIES

A. Berry curvature

The dependence of the internal structure of electrons on the dynamical parameter may result in anomalous transport properties, such as the Berry-phase effect [1,35,50–53]. Indeed, the Berry phase is marked by the Berry curvature, which is equivalent to an effective magnetic field in k space. The Berry curvature $\mathbf{\Omega}_n(\mathbf{k})$ is nonzero for crystals with either time reversal or broken inversion symmetries. Note that the Berry curvature is an odd function in the presence of time reversal symmetry and even in the presence of inversion symmetry [3,34,54], so that it has opposite signs in opposite valleys. Similarly, the valence and conduction bands have opposite Berry curvatures $\mathbf{\Omega}_v(\mathbf{k}) = -\mathbf{\Omega}_c(\mathbf{k})$. In general, the exciton wave function in ML TMDC is sharply localized in momentum space; then we can approximate $\mathbf{\Omega}_n(\mathbf{k})$ with its value at the band edge. For all four compounds MX_2, $\mathbf{\Omega}(k = 0)$ is about 15 Å^2 [1].

The dependence of the internal structure of the trion wave function on the center-of-mass wave vector can give rise to a gauge structure similar to that of the electron [52]. For example, the positive trion is made up of two holes that occupy the topmost valence band subbands and one electron. Figure 3 shows the various spin and valley configurations of positive trions. We schematize only those with the electron in the K valley; the two other configurations are time reversal counterparts of the ones listed. The positive (negative) trion acquires a Berry curvature given by the sum of the Berry curvatures of the two holes (electrons) and electron (hole) constituents. As the Berry curvatures from the two holes (electrons) in opposite valleys cancel, the positive (negative) trion Berry curvature is determined by the electron (hole) constituent. As a result, the two valley configurations of the positive (negative) trion have opposite Berry curvatures.

The intervalley trions as composite particles can acquire valley-dependent Berry curvature from the inheritance of the Berry curvature from the Bloch band and from the Coulomb exchange interaction between the carrier constituents. We

recall that the long range of the intravalley and intervalley exchange contributions, which leads to an energy shift, vanishes at the K and K' points of the Brillouin zone. Contrariwise, the electron-hole exchange interaction δ^{exch} gives rise to splitting between intravalley and intervalley negative-trion states [14,38]. For the positive trion, as well as the MoX_2 family, the exchange interaction leads to only a trivial energy shift at $\mathbf{K}+\mathbf{k}$. However, the negative intervalley trions in WX_2 can acquire valley-dependent Berry curvature originating from the Coulomb exchange interaction, in addition to that given by the Bloch bands. In the context of valley trions, to obtain the Berry curvature with center-of-mass wave vector $\mathbf{K}+\mathbf{k}$, we will calculate the corresponding normalized eigenvectors for the spinor part of Eq. (6):

$$\begin{aligned} |u_{s,+}(k)\rangle &= \cos(\alpha/2)|+\rangle - \sin(\alpha/2)e^{2i\beta}|-\rangle, \\ |u_{s,-}(k)\rangle &= \sin(\alpha/2)e^{-2i\beta}|+\rangle + \cos(\alpha/2)|-\rangle, \end{aligned} \tag{8}$$

where $\alpha(k)$ and $\beta(k)$ are the azimuthal and polar angles on the Bloch sphere, respectively, such that $\tan(\alpha) = 2|J^{inter}_{e-h}|/\delta^{\text{exch}}$ [55]. The Hilbert space is spanned by the pseudospins described by the spin-up (spin-down) state $|+\rangle$ ($|-\rangle$) [47]. In order to evaluate the valley trion properties, the Berry connection $\mathbf{A}_\varsigma(\mathbf{k})$ and Berry curvature $\mathbf{\Omega}_\varsigma(\mathbf{k})$, are defined, respectively, as

$$\mathbf{A}_\varsigma(\mathbf{k}) = \langle u_\varsigma(\mathbf{k})|i\nabla_{\mathbf{k}}|u_\varsigma(\mathbf{k})\rangle, \tag{9}$$

$$\mathbf{\Omega}_\varsigma(\mathbf{k}) = \nabla_{\mathbf{k}} \times \mathbf{A}_\varsigma(\mathbf{k}). \tag{10}$$

$\mathbf{A}_\varsigma(\mathbf{k})$ and $\mathbf{\Omega}_\varsigma(\mathbf{k})$ are equivalent to a vector potential and magnetic field in the valley trion center-of-mass momentum space, respectively. The integral of $\mathbf{\Omega}_\varsigma(\mathbf{k})$ over the k-space area gives rise to the Berry phase of the valley trion. Using Eq. (8) in Eq. (10), we obtain $\mathbf{\Omega}_\varsigma(\mathbf{k}) = [\nabla_{\mathbf{k}}\cos(\alpha) \times \nabla_{\mathbf{k}}\beta]\varsigma/2$. For the intervalley trion in ML WX_2, i.e., subjected to exchange electron-hole interaction, one finds the Berry curvature:

$$\Omega^{\text{exch}}(k) = -\sigma_z \frac{2J^2}{(\delta^{\text{exch}}K)^2} \times \frac{k_s^3}{(k_s+k)^3}\left(1+\frac{4J^2k_s^2}{(\delta^{\text{exch}}K)^2}\frac{k^2}{(k+k_s)^2}\right)^{-3/2}. \tag{11}$$

Here, $J \approx |\phi_{\tilde{1}s}(0)|^2(at/E_g)^2Ke^2/(\varepsilon_{\text{sub}}+\varepsilon_{\text{cap}})$. We notice that, for $J=0$, the Berry curvature vanishes and diverges at the Dirac points. The Berry curvature is concentrated in the two inequivalent valleys and has opposite signs in K and K', as shown in Fig. 4. In such a structure, upon the application of an electric field, the valley Hall effect is induced. The valley transport in systems with broken inversion symmetry provides a pathway to potential valley-based electronic applications [53]. The effect of the Berry phase manifests through not only the Berry curvature but also the orbital magnetic moment; the latter is the purpose of the following section.

B. Orbital moment

The orbital moment is an intrinsic property of the valence and conduction bands. Since the orbital moment depends on the valley, the coupling of magnetic field to the valley pseudospin and the detection of valley polarization as a magnetic signal are possible. In addition to the spin magnetic moment, Bloch electrons carry an orbital magnetic moment [34], which results from the self-rotation of the wave packet. Like the Berry curvature in ML TMDC, the orbital magnetic moment is in the normal direction of the plane. For a two-band model with particle-hole symmetry [34], the Berry curvature and the orbital magnetic moment are related by the following formula: $\mathbf{m}(k) = \xi(k)\mathbf{\Omega}(k)e/\hbar$. The orbital magnetic moment decreases going away from Dirac points K and K'. A nonzero orbital magnetic moment suggests that the valley carriers possess optical circular dichroism. Similar to the Berry curvature, the orbital magnetic moment acquires an additional term arising from the exchange interaction. For $k \simeq \mathbf{K}$, this term is given by $\mathbf{m}^{\text{exch}}(k) = \delta^{\text{exch}}\mathbf{\Omega}^{\text{exch}}(k)e/2\hbar$, as shown in the inset of Fig. 4. The moment can be used as an effective way to detect and generate the valley polarization [34].

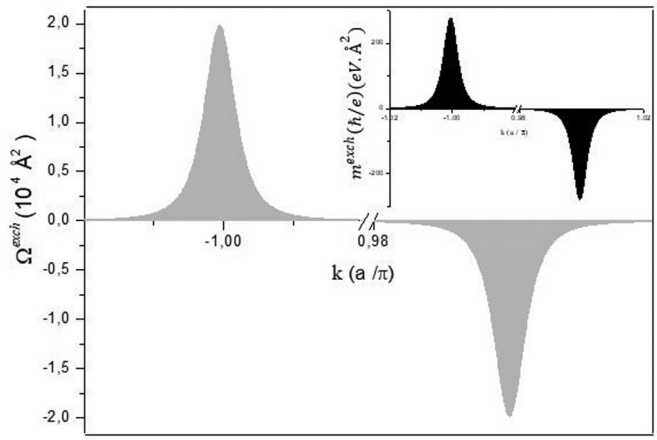

FIG. 4. The Berry curvature $\Omega^{\text{exch}}(k)$ as a function of the center-of-mass trion wave vector for $k_s = 0.15$ Å^{-1} and $\varepsilon_{\text{sub}} = \varepsilon_{\text{cap}} = 3.3$. The trion fine structure gives rise to a large pseudospin valley-dependent Berry curvature with a peak value of $\sim 10^4$ Å^2 in the K and K' valleys. The orbital magnetic moment $m^{\text{exch}}(k)$ has a distribution similar to that of $\Omega^{\text{exch}}(k)$, as shown in the inset.

The signal of the orbital magnetization M, arising from the summation of the orbital moment and the Berry curvature, may be used to distinguish between the two valleys; $\mathbf{M}$ is expressed as follows [34,53]:

$$\mathbf{M} = \frac{1}{2\pi^2}\int kdk\{\mathbf{m}(\mathbf{k}) + [\mu_c - \xi(k)]\mathbf{\Omega}^T(k)e/\hbar\}; \tag{12}$$

the integration is over states below the local chemical potential μ_c. Here, $\Omega^T = \Omega^{\text{exch}}(k) + \Omega(k)$ is the total trion Berry curvature, where $\Omega(k) = \Omega^e(k) + \Omega^h(k) + \Omega^{e/h}(k)$ is the Berry curvature driven by the Berry phase which is associated with the Bloch electrons. Note that, for a positive trion $\Omega^{\text{exch}}(k) = 0$; thus, $\Omega^T(k) = \Omega^e(k)$. In addition to the self-rotation of the wave packet, the orbital magnetization has another contribution which is due to the center-of-mass motion. Equation (12) can be further simplified as $\frac{\hbar}{e}\mathbf{M} = \frac{1}{\pi}\int kdk\mu_c\mathbf{\Omega}^T(k)$. In Fig. 5, we show the simultaneous impact of the exciton reduced mass μ and the screening parameter k_s on the magnetization. The shape of the graph is dictated by the dependence of the electron-hole oscillator strength [49]

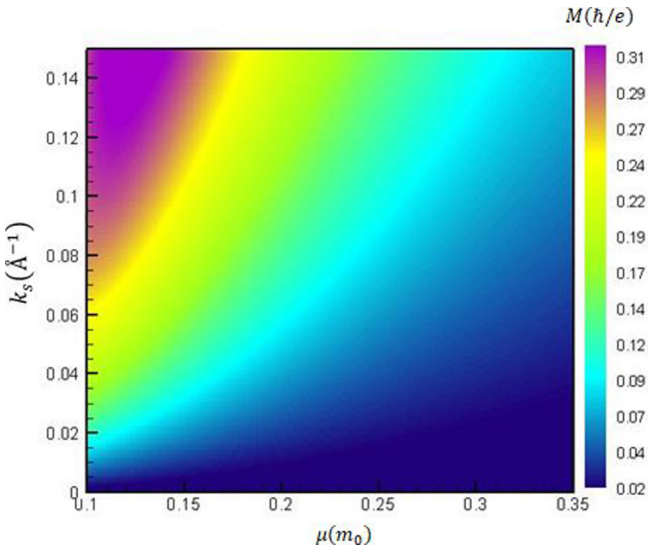

FIG. 5. The variation of the magnetization M as a function of the screening parameter k_s and reduced mass μ, showing the giant Berry curvature effect on the intervalley negative trion in a hBN-encapsulated WX_2 ML.

$|\phi_{\tilde{1}s}(0)|^2$ on the exciton reduced mass, substrate, and screening length. Analytically, the magnetization is enhanced by the chemical potential. At fixed carrier density around 10^{12} cm^{-2}, the calculated magnetization of a negative trion in ML WX_2 encapsulated in hBN, illustrated in Fig. 5, is summarized in Table I. As μ and k_s are not precisely known, one may deduce that M is easily detectable for large k_s and light reduced mass. As an example, using the parameters given by Courtade *et al.* [8], M is approximately ten times more intense than that calculated with the parameters extracted from Goryca *et al.* [56]. For a given sample, we can conclude that M is sensitive to the reduced mass, screening length, and surrounding dielectric environment. The magnetization can be related to the Hall conductivity through the relation $M \propto \mu_c \sigma$. These results offer the possibility to tune M and σ by external parameters like dielectric environment, doping, and reduced mass (choice of material).

C. Anomalous Hall effect

There are different contributions to the anomalous Hall effect [53]; the extrinsic contributions originate from the skew and side-jump scattering and the intrinsic contribution [60,61]. The skew scattering results from the scattering amplitude for spin/valley electrons. The side-jump contribution [62–64] is related to the shift of the wave packet at the scattering from the impurity. The intrinsic contribution, which is independent of scattering, originates from the Berry phase [65]. The anomalous velocity induced by the giant Berry curvature arising from the trion fine structure is our interest.

We recall that, due to the inversion symmetry breaking, the K and K' valleys exhibit valley contrast for the Berry curvature. By applying an in-plane electric field, a valley Hall current is observed [66]. As an experimental setup, an external electric field can be achieved by a gate voltage. Therefore, due to the presence of the Berry curvature, an electron wave packet moving through the region of electric field will acquire an anomalous term perpendicular to the direction of the applied electric field. Then, the Berry curvature modifies the electron dynamics. With a finite Berry curvature, the equations of motion are noncanonical [53–55], which leads to the violation of Liouville's theorem. The semiclassical equations of motion for Bloch electrons in weak electric **E** and magnetic fields **B** are

$$\hbar\dot{\mathbf{R}} = \frac{\partial E_n(\mathbf{k})}{\partial \mathbf{k}} - \hbar\dot{\mathbf{k}} \times \mathbf{\Omega}_n(\mathbf{k}), \tag{13}$$

$$\hbar\dot{\mathbf{k}} = -e\mathbf{E}(\mathbf{R}) - e\dot{\mathbf{R}} \times \mathbf{B}(\mathbf{R}). \tag{14}$$

$\mathbf{\Omega}_n(\mathbf{k})$ gives rise to an anomalous velocity perpendicular to an external electric field. Such a phenomenon is called the anomalous Hall effect. As previously mentioned, the bright positive (negative) trions have opposite Berry curvatures, thus leading to the valley Hall effect. Upon the recombination of the positive (negative) trion, the hole (electron) left behind is valley and spin polarized. Therefore, the trion valley Hall effect may be used for the generation of valley and spin polarizations of both electrons and holes. Especially, the large negative-trion valley Hall effect can be detected from a spatially dependent PL polarization model, as shown in Fig. 6.

It is interesting to note that, at low temperature and in a clean sample, the large valley Hall effect resulting from the giant Berry curvature cannot be compensated by the side-jump one. In addition, the Berry curvature of the negative intervalley trion, induced from the exchange, facilitates the valley Hall effect measurement. In comparison to an experiment using excitons [67,68], with charged excitons we do not need ionization of the optically generated electron-hole pair.

The above semiclassical equation of motion given by Eq. (13) is the basis for calculation of trion transport currents driven by an applied electric field. Under an in-plane electric field, the bright intervalley trions acquire opposite transverse velocities due to the exciton pseudospin valley-dependent Berry curvature. The trion will move to the two opposite boundaries of the sample, leading to a Hall current of valleys, spins, and charges. The Hall trion current density, driven by

TABLE I. The intervalley trion magnetization for both WSe2 and WS_2 MLs encapsulated by hBN.

	WSe_2					WS_2			
$\mu(m_0)$	0.2 [56,57]	0.16 [8]	0.18 [8]	0.16 [58]	0.16 [58]	0.175 [56]	0.15 [59]	0.15 [59]	0.15 [59]
r_s (Å)	45 [56,57]	6.4 [8]	13.6 [8]	50 [58]	9.38 [58]	34 [56]	30 [59]	40 [59]	50 [59]
k_s (Å^{-1})	0.02	0.15	0.073	0.02	0.106	0.029	0.033	0.025	0.02
M [meV $(e/\hbar)$]	38	299	143	53	232	64	96	74	60

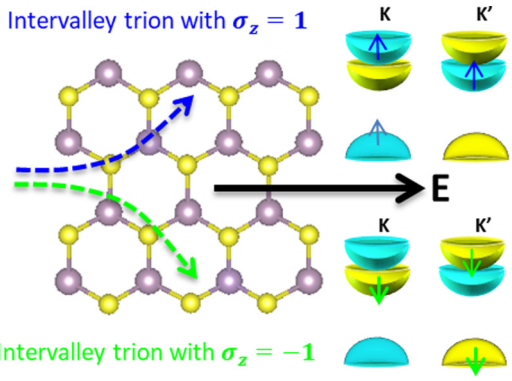

FIG. 6. Schematic of the valley Hall effect of bright intervalley trions in ML WX_2. By the application of an in-plane electric field **E**, trions which are distinguished by σ_z will move to the opposite edges of the sample and acquire a spatially dependent polarization model.

mechanical force, can be defined as [69]

$$J^H = -\frac{e}{4\pi^2}\int d\mathbf{k} f(\mathbf{k},\mathbf{R})\dot{R}, \tag{15}$$

where $f(\mathbf{k},\mathbf{R})$ is the distribution function and the integration is over states below the chemical potential. The combination of the semiclassical equations of motion with the Boltzmann equation gives us

$$J^H = -E\frac{e^2}{4\pi^2\hbar}\int d\mathbf{k} f(\mathbf{k})\Omega^T(\mathbf{k}). \tag{16}$$

The Hall current originates mainly from the equilibrium part of the carrier distribution and is known as the intrinsic contribution. Hence, we deduce the trion intrinsic Hall conductivity, which is expressed as [52,70]

$$\sigma^{\text{int}} = \frac{e^2}{4\pi^2\hbar}\int d\mathbf{k} f(\mathbf{k})\Omega^T(\mathbf{k}). \tag{17}$$

The dependence of the Berry curvature on the valley pseudospin σ_z, given by Eq. (11), engenders a valley Hall conductivity, expressed as follows:

$$\sigma^v = -\sigma_z\frac{4e^2J^2k_s^3}{\pi\hbar(\delta^{\text{exch}}K)^2}\int\frac{kdkf(k)}{(k_s+k)^3} \times\left(1+\frac{4J^2k_s^2}{(\delta^{\text{exch}})^2K^2}\frac{k^2}{(k+k_s)^2}\right)^{-3/2}. \tag{18}$$

The exchange-induced Berry curvature of trions should make the valley Hall effect easier to achieve. In Fig. 7, we plot the variation of the anomalous valley Hall conductivity as a function of the screening parameter k_s and the electron density. For a weak screening parameter k_s, the valley Hall conductivity increases slowly as a function of the density. For a fixed average dielectric constant of the surrounding material ε, the electron-hole exchange interaction δ^{exch} increases with increasing k_s. Consequently, the Berry curvature, magnetization, and Hall conductivity increase. For a large k_s ($r_s = 1/k_s \to 0 \Rightarrow k_s \to \infty$), the Rytova-Keldysh potential given by Eq. (7) is equivalent to the conventional Coulomb

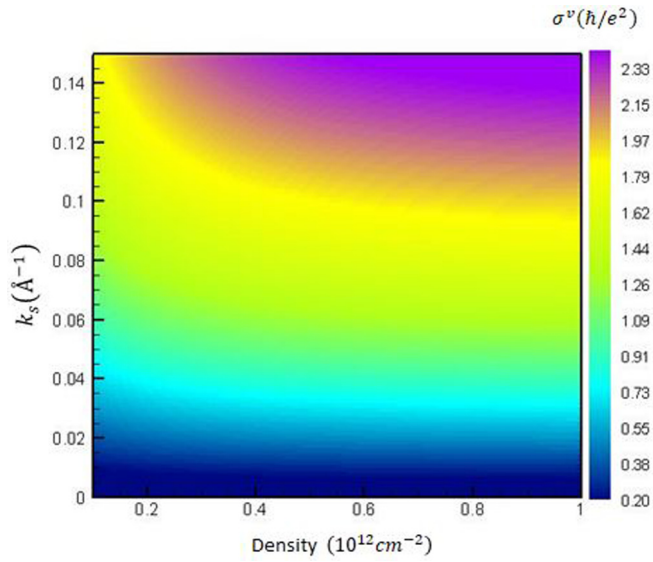

FIG. 7. Doping and screening parameter dependence of the anomalous trion valley Hall conductivity in hBN-encapsulated WSe_2 ML.

interaction. Equation (18) is integrated to give, at $T = 0$,

$$\sigma^v(k_s\to\infty) = -\sigma_z\frac{4\pi e^2}{\hbar}\left(1-\frac{1}{\sqrt{1+4J^2k_F^2/(\delta^{\text{exch}})^2K^2}}\right), \tag{19}$$

where k_F is the Fermi wave vector. For $J = 0$, the valley Hall conductivity originates from the exchange vanishing, whereas for $\delta^{\text{exch}} = 0$, $\sigma^v(k_s\to\infty) = 4\pi e^2/\hbar$. Finally, trions as charged excitons influence both transport and optical properties and may be manipulated and detected in many experiments such as the valley Hall effect. This allows the trion to play an important role in manipulating electron spin and the valley degree of freedom [33].

IV. CONCLUSION

In this paper, we have investigated the negative-trion fine structure in a high-quality ML WX_2. We have shown that, due to the electron-hole exchange interaction, the intervalley spin-triplet trion and intravalley spin-singlet trion are separated by an energy splitting of around 6 meV. Thanks to the broken inversion symmetry in ML TMDC and the trion fine structure, the Berry curvature gives rise to a large anomalous valley Hall effect which can be used to detect and generate valley polarization by an electric field. Using the semiclassical equations of motion, we have shown that the valley Hall conductivity due to the giant Berry curvature arising from the trion fine structure and the magnetization are tunable and controlled by external parameters and material parameters, such as the exciton reduced mass and dielectric screening length.

ACKNOWLEDGMENT

We thank M. O. Goerbig for critically reading the manuscript.

[1] D. Xiao, G. B. Liu, W. Feng, X. Xu, and W. Yao, Phys. Rev. Lett. **108**, 196802 (2012).

[2] A. M. Jones, H. Yu, N. J. Ghimire, S. Wu, G. Aivazian, J. S. Ross, B. Zhao, J. Yan, D. G. Mandrus, D. Xiao, W. Yao, and X. Xu, Nat. Nanotechnol. **8**, 634 (2013).

[3] X. Xu, W. Yao, D. Xiao, and T. F. Heinz, Nat. Phys. **10**, 343 (2014).

[4] H. Yu, G. Liu, P. Gong, X. Xu, and W. Yao, Nat. Commun. **5**, 3876 (2014).

[5] A. Chernikov, T. C. Berkelbach, H. M. Hill, A. Rigosi, Y. Li, O. B. Aslan, D. R. Reichman, M. S. Hybertsen, and T. F. Heinz, Phys. Rev. Lett. **113**, 076802 (2014).

[6] Z. Ye, T. Cao, K. O'Brien, H. Zhu, X. Yin, Y. Wang, S. G. Louie, and X. Zhang, Nature (London) **513**, 214 (2014).

[7] P. Tonndorf, R. Schmidt, R. Schneider, J. Kern, M. Buscema, G. A. Steele, A. Castellanos-Gomez, H. S. J. van der Zant, S. Michaelis de Vasconcellos, and R. Bratschitsch, Optica **2**, 347 (2015).

[8] E. Courtade, M. Semina, M. Manca, M. M. Glazov, C. Robert, F. Cadiz, G. Wang, T. Taniguchi, K. Watanabe, M. Pierre, W. Escoffier, E. L. Ivchenko, P. Renucci, X. Marie, T. Amand, and B. Urbaszek, Phys. Rev. B **96**, 085302 (2017).

[9] A. Raja, A. Chaves, J. Yu, G. Arefe, H. M. Hill, A. F. Rigosi, T. C. Berkelbach, Ph. Nagler, C. SchuÂ¨ller, T. Korn, C. Nuckolls, J. Hone, L. E. Brus, T. F. Heinz, D. R. Reichman, and A. Chernikov, Nat. Commun. **8**, 15251 (2017).

[10] M. R. Molas, K. Nogajewski, A. Slobodeniuk, J. Binder, M. Bartos, and M. Potemski, Nanoscale **9**, 13128 (2017)

[11] M. R. Molas, C. Faugeras, A. O. Slobodeniuk, K. Nogajewski, M. Bartos, D. M. Basko, and M. Potemski, 2D Mater. **4**, 021003 (2017).

[12] M. Szyniszewski, E. Mostaani, N. D. Drummond, and V. I. Falko, Phys. Rev. B **95**, 081301(R) (2017).

[13] G. Wang, A. Chernikov, M. M. Glazov, T. F. Heinz, X. Marie, T. Amand, and B. Urbaszek, Rev. Mod. Phys. **90**, 21001 (2018).

[14] D. Vaclavkova, J. Wyzula, K. Nogajewski, M. Bartos, A. O. Slobodeniuk, C. Faugeras, M. Potemski, and M. R. Molas, Nanotechnology **29**, 325705 (2018).

[15] M. Trushin, M. O. Goerbig, and W. Belzig, Phys. Rev. Lett. **120**, 187401 (2018).

[16] A. V. Stier, N. P. Wilson, G. Clark, X. Xu, and S. A. Crooker, Nano Lett. **16**, 7054 (2016).

[17] M. Van der Donck, M. Zarenia, and F. M. Peeters, Phys. Rev. B **96**, 035131 (2017).

[18] T. Cao, G. Wang, W. Han, H. Ye, C. Zhu, J. Shi, Q. Niu, P. Tan, E. Wang, B. Liu, and J. Feng, Nat. Commun. **3**, 887 (2012).

[19] G. Wang, L. Bouet, D. Lagarde, M. Vidal, A. Balocchi, T. Amand, X. Marie, and B. Urbaszek, Phys. Rev. B **90**, 075413 (2014).

[20] A. T. Hanbicki, M. Currie, G. Kioseoglou, A. L. Friedman, and B. T. Jonker, Solid State Commun. **203**, 16 (2015).

[21] A. V. Stier, K. M. McCreary, B. T. Jonker, J. Kono, and S. A. Crooker, Nat. Commun. **7**, 10643 (2016).

[22] A. Hichri, I. Ben Amara, S. Ayari, and S. Jaziri, J. Appl. Phys. **121**, 235702 (2017); J. Phys.: Condens. Matter **29**, 435305 (2017).

[23] M. Danovich, V. Zólyomi, and V. I. Falko, Sci. Rep. **7**, 45998 (2017).

[24] G. Gupta, S. Kallatt, and K. Majumdar, Phys. Rev. B **96**, 081403(R) (2017).

[25] J. Jadczak, J. Kutrowska-Girzycka, P. Kapuciski, Y. S. Huang, A. Wójs, and L. Bryja, Nanotechnology **28**, 395702 (2017).

[26] I. Kylänpää and H.-P. Komsa, Phys. Rev. B **92**, 205418 (2015).

[27] T. Jakubczyk, K. Nogajewski, M. Molas, M. Bartos, W. Langbein, M. Potemski, and J. Kasprzak, 2D Mater. **5**, 031007 (2018).

[28] G. Plechinger, P. Nagler, A. Arora, R. Schmidt, A. Chernikov, A. Granados del Aguila, P. C. M. Christianen, R. Bratschitsch, C. Schuller, and T. Korn, Nat. Commun. **7**, 12715 (2016).

[29] Z. Li, T. Wang, S. Miao, Z. Lian, and S. F. Shi, Nanophotonics **9**, 1811 (2020).

[30] A. Jones, H. Yu, J. Schaibley, J. Yan, D. G. Mandrus, T. Taniguchi, K. Watanabe, H. Dery, W. Yao, and X. Xu, Nat. Phys. **12**, 323 (2016).

[31] G. Aivazian, Z. Gong, A. M. Jones, R. L. Chu, J. Yan, D. G. Mandrus, C. Zhang, D. Cobden, W. Yao, and X. Xu, Nat. Phys. **11**, 148 (2015).

[32] J. R. Schaibley, H. Yu, G. Clark, P. Rivera, J. S. Ross, K. L. Seyler, W. Yao, and X. Xu, Nat. Rev. Mater. **1**, 16055 (2016).

[33] A. Singh, G. Moody, K. Tran, M. E. Scott, V. Overbeck, G. Berghauser, J. Schaibley, E. J. Seifert, D. Pleskot, N. M. Gabor, J. Yan, D. G. Mandrus, M. Richter, E. Malic, X. Xu, and X. Li, Phys. Rev. B **93**, 41401(R) (2016).

[34] D. Xiao, W. Yao, and Q. Niu, Phys. Rev. Lett. **99**, 236809 (2007).

[35] W. Yao, D. Xiao, and Q. Niu, Phys. Rev. B **77**, 235406 (2008).

[36] H. M. Price, T. Ozawa, and I. Carusotto, Phys. Rev. Lett. **113**, 190403 (2014).

[37] M. C. Chang and Q. Niu, J. Phys.: Condens. Matter **20**, 193202 (2008).

[38] H. Yu, X. Cui, X. Xu, and W. Yao, Nat. Sci. Rev. **2**, 57 (2015).

[39] A. Srivastava, M. Sidler, A. V. Allain, D. S. Lembke, A. Kis, and A. Imamoglu, Nat. Phys. **11**, 141 (2015).

[40] N. Nagaosa, J. Sinova, S. Onoda, A. H. MacDonald, and N. P. Ong, Rev. Mod. Phys. **82**, 1539 (2010).

[41] N. S. Rytova, arXiv:1806.00976v1.

[42] A. Hichri, S. Jaziri, and M. O. Goerbig, Phys. Rev. B **100**, 115426 (2019).

[43] T. P. Lyons, S. Dufferwiel, M. Brooks, F. Withers, T. Taniguchi, K. Watanabe, K. S. Novoselov, G. Burkard, and A. I. Tartakovskii, Nat. Commun. **10**, 2330 (2019).

[44] X.-X. Zhang, Y. You, Shu Zhao, and T. F. Heinz, Phys. Rev. Lett. **115**, 257403 (2015).

[45] E. Mostaani, M. Szyniszewski, C. H. Price, R. Maezono, M. Danovich, R. J. Hunt, N. D. Drummond, V. I. Falko, Phys. Rev. B **96**, 075431 (2017).

[46] See Supplemental Material at http://link.aps.org/supplemental/10.1103/PhysRevB.102.085407, which includes Refs. [71,72], for a detailed calculation of electron-hole exchange interaction of a negative trion in ML WX_2.

[47] Z. R. Gong, W. Z. Luo, Z. F. Jiang, and H. C. Fu, Sci. Rep. **7**, 42390 (2017).

[48] S. Y. Chen, T. Goldstein, J. Tong, T. Taniguchi, K. Watanabe, and J. Yan, Phys. Rev. Lett. **120**, 046402 (2018).

[49] I. Ben Amara, A. Hichri, and S. Jaziri, J. Phys.: Condens. Matter **29**, 505302 (2017).

[50] D. Xiao, J. Shi, and Q. Niu, Phys. Rev. Lett. **95**, 137204 (2005).

[51] D. Xiao, Y. Yao, Z. Fang, and Q. Niu, Phys. Rev. Lett. **97**, 026603 (2006).
[52] W. Yao and Q. Niu, Phys. Rev. Lett. **101**, 106401 (2008).
[53] D. Xiao, M. C. Chang, and Q. Niu, Rev. Mod. Phys. **82**, 1959 (2010).
[54] J. Zhou, W. Y. Shan, W. Yao, and D. Xiao, Phys. Rev. Lett. **115**, 166803 (2015).
[55] J. N. Fuchs, F. Piéchon, M. O. Goerbig, and G. Montambaux, Eur. Phys. J. B **77**, 351 (2010).
[56] M. Goryca, J. Li, A. V. Stier, T. Taniguchi, K. Watanabe, E. Courtade, S. Shree, C. Robert, B. Urbaszek, X. Marie, and S. A. Crooker, Nat. Commun. **10**, 4172 (2019).
[57] A. V. Stier, N. P. Wilson, K. A. Velizhanin, J. Kono, X. Xu, and S. A. Crooker, Phys. Rev. Lett. **120**, 057405 (2018).
[58] D. Van Tuan, M. Yang, and H. Dery, Phys. Rev. B **98**, 125308 (2018).
[59] J. Zipfel, J. Holler, A. A. Mitioglu, M. V. Ballottin, P. Nagler, A. V. Stier, T. Taniguchi, K. Watanabe, S. A. Crooker, P. C. M. Christianen, T. Korn, and A. Chernikov, Phys. Rev. B **98**, 075438 (2018).
[60] R. Karplus and J. M. Luttinger, Phys. Rev. **95**, 1154 (1954).
[61] M. I. Dyakonov and A. V. Khaetskii, in *Spin Physics in Semiconductors*, 2nd ed., edited by M. I. Dyakonov, Springer Series in Solid-State Sciences Vol. 157 (Springer, 2017), Chap. 8.
[62] L. Berger, Phys. Rev. B **2**, 4559 (1970).
[63] N. A. Sinitsyn, Q. Niu, and A. H. MacDonald, Phys. Rev. B **73**, 075318 (2006).
[64] N. A. Sinitsyn, J. Phys.: Condens. Matter **20**, 023201 (2008).
[65] N. A. Sinitsyn, Q. Niu, J. Sinova, and K. Nomura, Phys. Rev. B **72**, 045346 (2005).
[66] N. Ubrig, S. Jo, M. Philippi, D. Constanzo, H. Berger, A. Kuzmenko, and A. Morpurgo, Nano Lett. **17**, 5719 (2017).
[67] K. F. Mak, K. L. McGill, J. Park, and P. L. McEuen, Science **344**, 1489 (2014).
[68] T. Mueller and E. Malic, 2D Mater Appl. **2**, 29 (2018).
[69] M.-C. Chang and Q. Niu, Phys. Rev. B **53**, 7010 (1996).
[70] A. Kormányos, V. Zólyomi, V. I. Fal'ko, and G. Burkard, Phys. Rev. B **98**, 035408 (2018).
[71] G. E. Pikus and G. L. Bir, Zh. Eksp. Teor. Fiz. **33**, 108 (1971).
[72] G. Fishman, *Semi-Conducteurs : Les Bases de la Théorie k.p* (Les éditions de l'école polytechnique, 2010), Vol. 1.